CERN-ATS-Note-2011-121 PERF

12. April 2012
Regina.Kwee@cern.ch

Commissioning and Operation of the H4IRRAD Mixed-Field Test Area

R. Kwee, B. Biskup, M. Brugger, M. Calviani, I. Efthymiopoulos, J. Mekki, F. La Torre, E. Lebbos, P. Mala, G. Manessi, A. Nordt, F. Pozzi, K. Roeed, C. Severino, M. Silari, A. Thornton

Keywords: Mixed-field calibration, BLM, RadMons, PIC, HEH, thermal neutron, Si 1 MeV neutron equivalent fluence, prompt dose, FLUKA simulations, LHC equipment testing

Summary

This note reports on the commissioning and operation period of the H4IRRAD Test Area in which well characterised mixed-fields are provided for LHC equipment users. In benchmark simulations the mixed-field components were estimated and measured with the H4IRRAD beam and radiation monitoring systems. The radiation monitors, the "RadMons" and beam-loss monitors (BLMs) are the same detector types used for monitoring radiation fluences in the underground areas of the LHC.

In the first two irradiation periods various equipment was exposed to irradiation produced by a secondary proton beam of 280 GeV impacting on the H4IRRAD copper target. Measurements compared to simulations are presented that quantify the high energy hadron, thermal neutron and Si 1 MeV neutron equivalent fluences at the given test locations. A crucial part was to calibrate the beam monitoring systems to measure the number of protons, p.o.t., which is outlined using different techniques. In addition, cross-checks of p.o.t. measurements are presented using the beam-loss-monitors which agree well within uncertainties.

Contents

1 Introduction

The LHC machine has achieved an highly performing state within the first two years of operation, providing to the general purpose experiments at the LHC more than[1] 4 fb^{-1} which almost 100 times as much as was delivered in the entire year 2010. This success is however accompanied by system and control failures of equipment along the LHC tunnel. A project called "Radiation to Electronics", R2E [1], has been created in 2009 to mitigate the risk of failures due to single-event-upsets (SEUs) of the control equipment installed in the tunnel and shielded areas. A definite mitigation plan has been setup for the upcoming operation stops. These will be used to relocate sensitive equipment or provide additional shielding where possible.

In order to determine the failure cross-section due to radiation of specific bulk equipment and special services that need high voltage powering and cooling systems a new test area has been setup in the H4-beamline of the North Area, H4IRRAD [2, 4, 3], in addition to the already present parasitic test area next to the CNGS experiment, CNRAD [5] which has major drawbacks for bulk equipment testing (limited access and essentially no control of the beam). Two well characterised mixed-fields are present at H4IRRAD, one similar to the radiation field present in the LHC tunnel (denoted in the following as *internal zone*) and another one that represents the shielded areas in the LHC underground areas (*external zone*). The test area has been setup during the first months of 2011 and has started operation in June 2011. Two time periods were analysed in which different LHC equipment was tested, the first one was in June 2011 from 12$^{\text{th}}$ to 28$^{\text{th}}$ and the second in July 2011 from 11$^{\text{th}}$ to 25$^{\text{th}}$. Results on the field characterisations are reported in this note.

2 The H4IRRAD Test Area

2.1 Layout

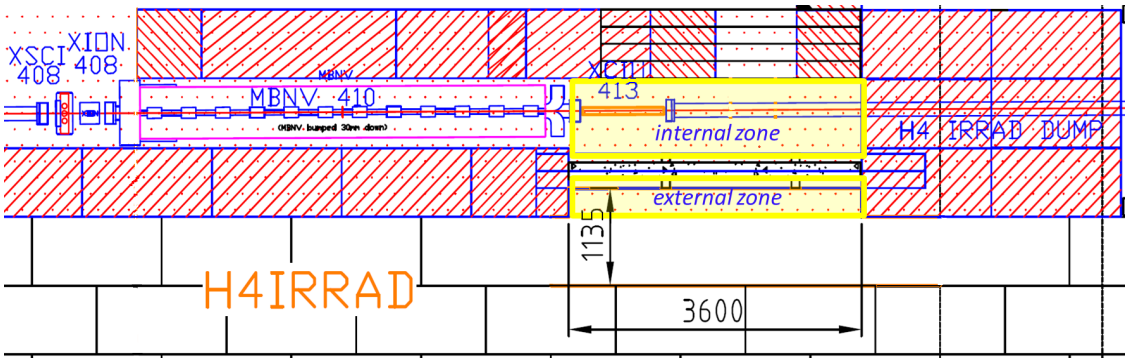

Figure 1: Extraction of a North Area drawing showing the layout of the H4IRRAD irradiation zones. The striped area represent iron blocks while the white ones are concrete blocks. Three beam monitor detectors on the H4IRRAD beamline are visible, scintillator 3 (XSCI) and the ionisation chamber (XION) at 408 m downstream of the T2 target. Scintillator 2 is placed 33 m upstream. At 413 m downstream of T2, the H4IRRAD copper target is installed.

An overview of the H4IRRAD-area is given in Fig.1 showing part of the H4-beamline, the internal zone with the H4IRRAD copper target and the external irradiation zone. A detailed description of the H4IRRAD installation can be found in [2]. The design of the geometry of the test area was

[1] Up to October 2011.

guided by results of FLUKA [6] simulations of expected radiation levels. Radiation fields in the in- and external irradiation locations as well as the influence of the inner shielding material composition and thickness were studied in the simulations. A 20 cm concrete inner shielding was chosen to produce a representative LHC-like shielded area. The main simulation results are presented in Section 2.2, a detailed report of the FLUKA studies is given in [7].

The external irradiation location was created by removing a few blocks of a concrete shielding and replacing the old iron shielding by the 20 cm thick concrete wall. For handling the tested equipment (installation and retrievement), a removable, 1.6 m thick iron roof was constructed. An iron beam dump was installed downstream of the H4IRRAD target area to safely absorb the full beam energy. Furthermore, shielding was properly extended at critical locations. Further installation details can be found in [2].

2.2 Expected Radiation Levels from Simulation

Table 1: Expected radiation levels at H4IRRAD from FLUKA simulations at different test locations as explained in the text. Values for prompt dose, HEH hadron fluence Φ_{HEH} and Si 1 MeV neutron equivalent fluence Φ_{neq} are indicated.

test location	prompt dose [Gy/week]	Φ_{HEH} [10^9/week/cm^2]	Φ_{neq} [10^9/week/cm^2]
internal zone A	13.6	22.1	102
external zone B	2.48	6.76	30.5
external zone C	2.57	6.22	19.9

Typical doses and particle fluences were simulated with FLUKA for which an SPS supercycle of 44 seconds was assumed with 10^9 protons per spill. The average prompt dose rate, high energy hadron fluence, Φ_{HEH}, and the Si 1 MeV neutron equivalent, Φ_{neq}, are shown in Fig. 3. For specific test locations in the internal and external zone (A: in internal zone downstream the H4IRRAD copper target, B and C: in external zone parallel to target and A-location, respectively) these fluences are listed in Table 1. Statistical uncertainties are not indicated as they are negligible compared to field gradients within the tested racks.

The Fig. 2 shows the prompt dose equivalent for various positions marked as #1 and #2 and located in *accessible areas* which are not permanent workplaces. The expected dose equivalent at position #1 and #2 are 0.6 $\pm$6 % and 0.04 $\pm$ 35 %, respectively. They thereby fulfill the requirements of a *supervised radiation area* for low-occupancy which shall not exceed 15 μSv/h [9]. The maximal prompt dose equivalent above the roof reaches the value of around 100 μSv/h and is thus not accessible during operation.

The muon fluence directly behind the iron dump is $3.3{\cdot}10^6$ muons/cm^2/week for a dose equivalent of 6.2 μSv/h. 850 cm further behind the H4IRRAD beam dump, the average muon fluence is reduced to $8.6 \cdot 10^5$ muons/cm^2/week corresponding to a dose equivalent of 1.6 μSv/h, which is sufficient to allow maintenance and other activities downstream the target area.

2.3 Beam Configuration

The primary beam is extracted from the SPS at 400 GeV and steered towards the T2 target with an intensity of $6 \cdot 10^{12}$ as illustrated in Fig. 4. The secondary beam has an energy of 280 GeV after T2 and passes various beam optics and collimators before it impacts on the H4IRRAD copper target

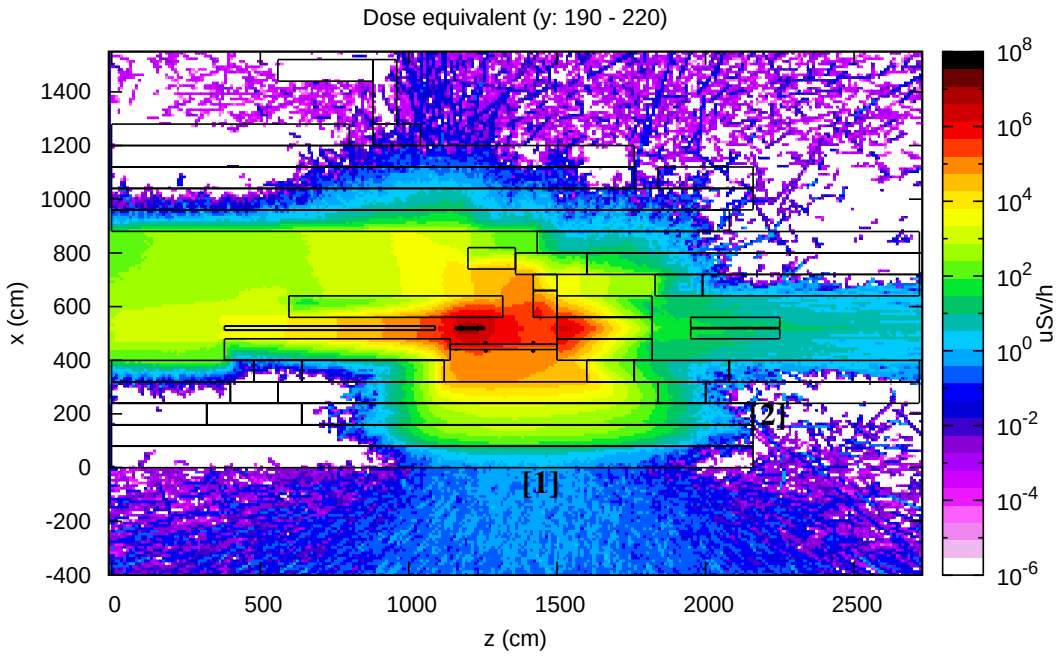

Figure 2: Horizontal projection of ambient dose equivalent in μSv/h for the H4IRRAD installation at nominal beam conditions. At position **1** and **2**, the expected dose equivalent was evaluated (see text).

Table 2: Beam composition of beam on T2. Numbers are taken from [8].

Particle	flux [part/p.o.t. Sr GeV]	content [%]	rate [particles/spill]
protons	86.54	94.27	$3.31 \cdot 10^8$
kaons	0.66	0.72	$2.52 \cdot 10^6$
pions	4.6	5.01	$1.76 \cdot 10^7$

with an intensity of $1 \cdot 10^9$ particles/pulse. Essentially protons are encountered at H4IRRAD with smaller contributions from pions and kaons, details are listed in Table 2.

2.4 Beam Profile

The accurate knowledge of the secondary beam profile is of paramount importance for the evaluation of the radiation field expected from the installation. Several measurements have been performed in order to determine it. During the commissioning phase, two photographic plates[2] were directly attached to end- and front side of the copper target. Two *filament scintillators*, FISC7 and FISC8 located at 402 m and 403 m downstream of T2 as shown in Fig. 4, are motorised wire scanners with a scintillation filament of 0.2 mm width. They were used to provide the horizontal and vertical profiles of the secondary proton beam, respectively.

Such a measurement of each FISC is shown in Fig. 5. While the shape of the vertical profile follows as expected a Gaussian, the horizontal shape exhibits a double-peak structure. This profile was considered in all FLUKA simulations. The horizontal profile is compared to the measurement by one of the photographic plate of the beam. A superposition of the beam image obtained by the

[2]One was Polaroid© film, the other a Gafchromic EBT2© Dosimetry film.

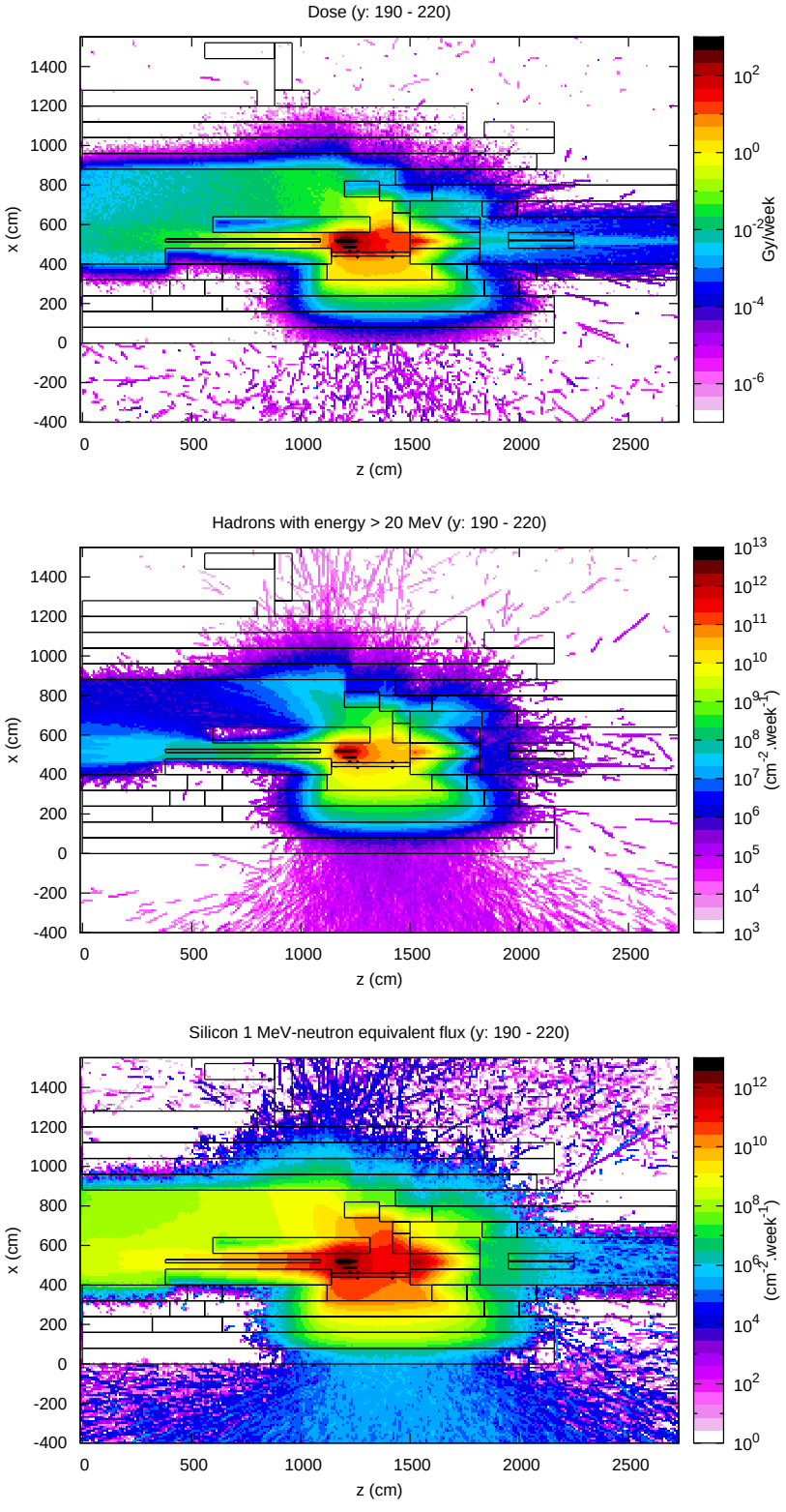

Figure 3: Horizontal projection of prompt dose (top), high energy hadron (middle) and Si 1 MeV neutron equivalent fluences (bottom) for the H4IRRAD installation at nominal beam conditions. Fluences at specific test locations in the internal and external zone are indicated in Table 1.

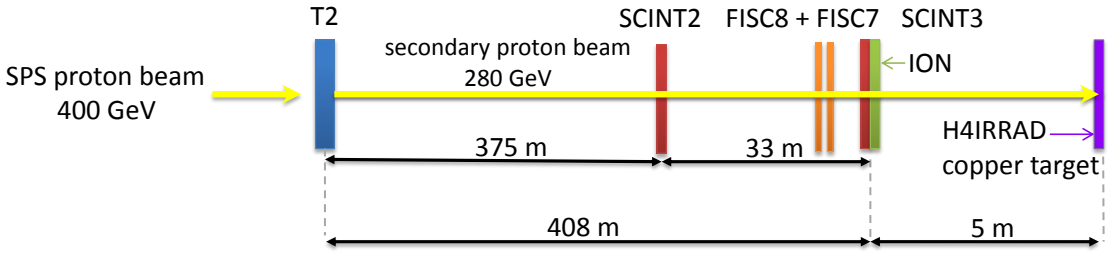

Figure 4: Sketch of H4IRRAD beam line showing the beam extraction from SPS on the T2 target to the H4IRRAD copper target. In the beamline, beam monitoring systems for H4IRRAD are placed (SCINT2, SCINT3 and ION, see text) and other instrumentation like two filament scintillators (FISCs) used to measure the beam profile.

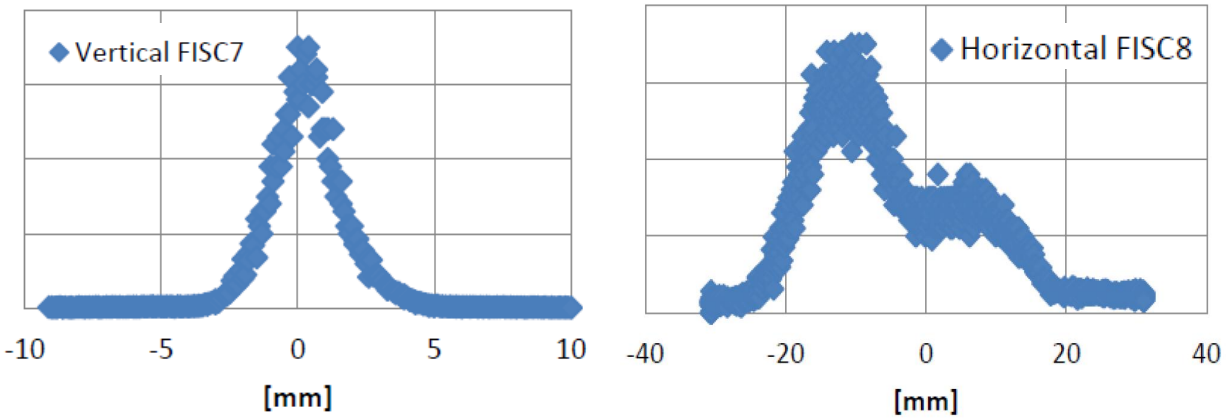

Figure 5: Wire-scanner results of FISC7 and FISC8 for vertical and horizontal profile measurement of the beam.

Polaroid film and the horizontal profile measured with FISC08 is depicted in Fig. 6. Due to the large exposure of the Polaroid film to a high intensity beam, it was not possible to obtain a quantitative evaluation of the beam intensity from the analysis of the image. Nevertheless, a good qualitative agreement was obtained.

3 Beam and Radiation Monitoring System

The beam monitoring system consists of three detector types which measure the number of charged particles. These are the ionisation chamber, denoted in the following as ION, two scintillators, SCINT2 and SCINT3, and a precision ionisation chamber, PIC. The radiation monitoring system measures radiation levels in terms of dose and high energy hadron fluences produced by the shower of particles created when the secondary proton beam hits the copper target of the installation. This monitoring system consists of beam loss monitors, BLM, and an online radiation field monitor, the RadMons system. These are the same type of radiation monitors that are used in critical zones of the LHC underground areas. Both, the beam and radiation monitoring systems are described in the following.

3.1 Ionisation Chamber – ION

The argon ionisation chamber as installed for the test area as shown in Fig 1 and 4, consists of a stainless steel cylinder (25 μm stainless steel), two thin end windows and 21 parallel electrodes of

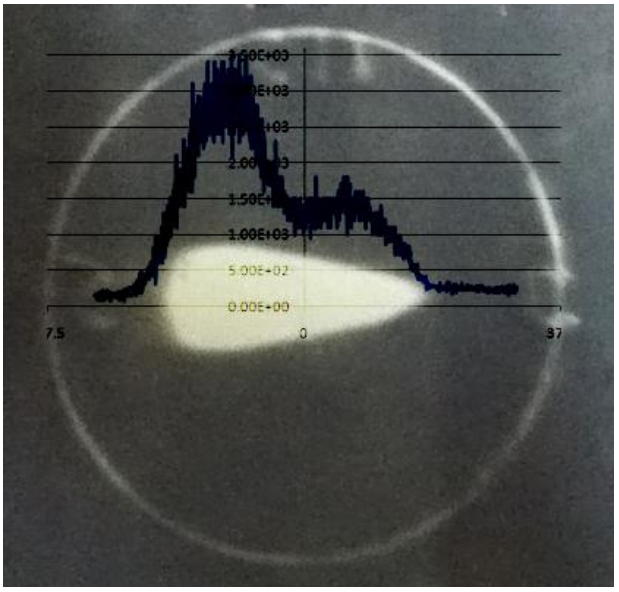

Figure 6: Superposition of beam profile measurements from FISC8 and the Polaroid film placed 6 m further downstream. One can observe that the extension of the horizontal shape is well conserved.

2 μm aluminum, The cylinder is filled with pure argon slightly above atmospheric pressure. It shows a linear response to particle fluxes ranging from 10^5 to 10^9 charged particles which bridges the range of scintillator counters and techniques for high fluxes e.g. based on foil activation. In addition, it shows very good long term stability and was therefore widely used in high intensity experiments, in particular those that use the CERN SPS and PS secondary beams. A detailed description is given in [11].

3.2 Scintillators – SCINT

Several plastic scintillators are installed in the North Area beamlines to monitor the secondary or tertiary beam intensities. The signal of two of them in coincidence are used for the beam monitoring in the H4IRRAD beamline. These are located at 375 m (SCINT2) and 408 m (SCINT3) downstream of the T2 target as sketched in Fig. 4 and a coincidence of them is in the remainder of the report denoted as SCINT. The scintillators have a diameter of 100 mm, are 4 mm thick and are sensitive to intensities ranging from 10^5 to 10^7 charged particles with very high efficiencies.

3.3 Precision Ionisation Chamber – PIC

The PIC is a precision ionisation chamber used since many years as a beam monitor at the CERF (CERN EU Reference Field) facility [12] in the H6 beam line. It is a simple parallel plate, transmission-type ionisation chamber with a diameter of 185 mm. The chamber has five parallel electrode plates made of Mylar of 2.5 mg/cm^2 thickness and 16 mm inter-plate spacing. The central plate is the collector and the ones on either side are the polarity electrodes. The voltage on these plates ($\sim$300 V) is guaranteed by an external battery. The PIC was mounted on a standard pedestal normally used to support beam line components such as vacuum chambers and was placed in the beam axis approximately two meters downstream from the center of the copper target (which had been removed when the PIC was operated in order to capture the full SPS proton beam). The signal coming from the chamber is fed into a charge digitizer which is mounted on the lower side of a base plate; this plate is mounted together with the PIC, sandwiched between the chamber and the pedestal. The

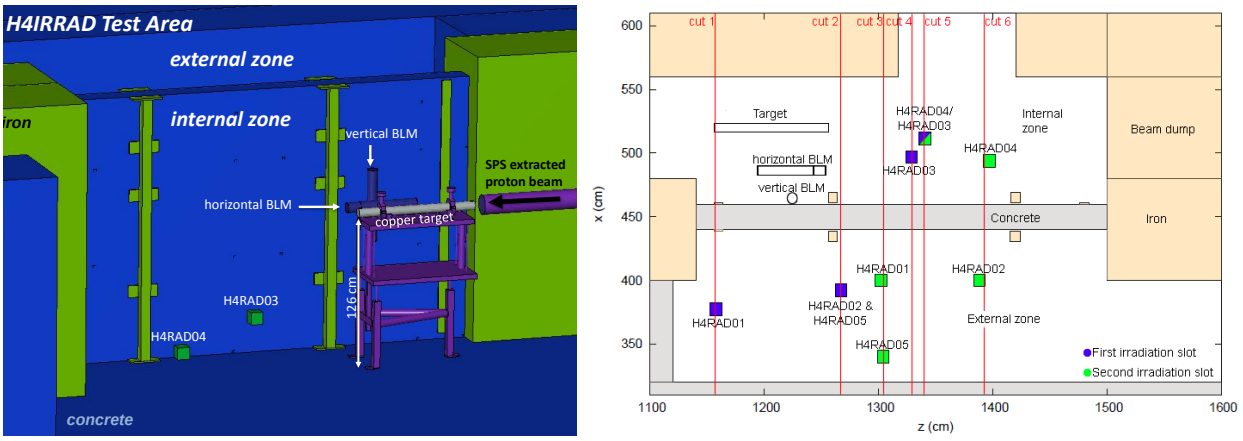

(a) (b)

Figure 7: (a) Radiation monitoring detectors (RadMons and BLMs) in the internal zone in a scenario during the 1^{st} irradiation period. (b) Top view of RadMon positions during the 1^{st} (blue) and 2^{nd} (green) irradiation periods. The vertical positions (six cut views) are shown in the Appendix in Fig. 12. Test equipment is not shown.

digitizer requires a 24 V voltage provided through a Burndy connector by an external power supply. The output pulses are fed to a National Instrument PCI 6602 acquisition card mounted on a desktop computer (PC). The reading of the PIC is acquired by a program written in LabVIEW [13].

3.4 Radiation Monitors – RadMons

Radiation Monitors, RadMons, are used in the LHC tunnel and shielded area as well as in the experimental caverns for online feedback on radiation levels [10, 16]. Around 330 of them are installed in the LHC where high radiation levels are expected [14]. They serve as an early warning system to protect the concerned electronic by measuring the total ionising dose on two different sensitivity levels (when biased at 3 and 5 V, respectively), Si 1 MeV neutron equivalent and hadron fluences. At H4IRRAD, five RadMons were used to estimate the hadron and neutron fluences, biased at both voltages, installed in the internal and external zones, see Fig. 7. The sensitivity of a RadMon corresponds to one count at both bias levels to roughly $2 \cdot 10^6$ HEH/cm^2, depending on the R-factor[3]. For detailed calculations, it is refered to [14]. At H4IRRAD, the RadMons have been placed at various positions in order to obtain measurements of several locations. This is depicted in Fig. 7 (b) and more detailed in the Appendix in Fig 12.

3.5 Beam Loss Monitoring Detectors – BLM

The LHC type of beam-loss-monitors (BLM) is a cylindric parallel-plate ionisation chamber of 50 cm length and 9 cm diameter. The sensitive part is 38 cm long, while the remaining volume is used for the readout electronics. 61 aluminum electrodes, 0.5 mm thick and measuring 7.5 cm in diameter, penetrate the nitrogen filling pressurised at 1.1 bar. Different bias voltages up to 1.5 kV are applied for an efficient charge collection.

In the LHC, the beam loss monitoring system consists of around 4000 BLM detectors [15]. Their task is to protect the superconducting elements from unwanted quenches by generating a beam abort trigger, if beam losses recognised as dose cumulated inside the chamber exceed a predefined threshold. Two of this kind are installed at H4IRRAD. One is horizontally aligned (hBLM), the

[3]The *risk factor* (R-factor) is the ratio of the thermal neutron fluence over the HEH fluence.

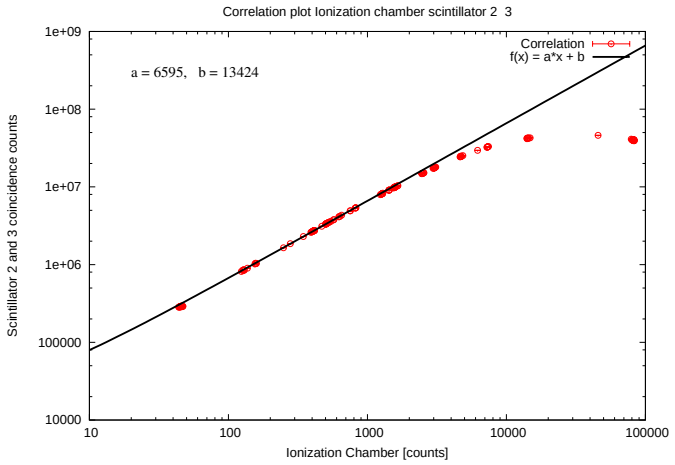

Figure 8: Calibration of ionisation chamber counts and coincidence counts of the scintillators during the first irradiation period.

other one vertically (vBLM) located at the same height of the copper target. The size of the BLMs combined with their location close to the secondary target, makes them extremely sensitive to the gradient of the radiation field. Both, the vertical and horizontal BLMs add up to the redundancy of the test area to measure the radiation fields allowing in addition to perform cross-checks on the measured number of protons/spill.

4 Calibration of Beam Monitoring

The calibration of beam monitoring consists in the determination of the number of protons, $N_{\text{p.o.t.}}$, impacting on the H4IRRAD target per SPS extraction. The detectors used for determining $N_{\text{p.o.t.}}$ are the scintillators, the ionisation chamber and the PIC. ION and SCINT cover different ranges of beam intensities, however with an overlapping region between a few 10^5 and 10^7 protons/spill in which both detectors give linear response. The calibration of the ION with the SCINT is described in Section 4.1. A cross-calibration was performed with the PIC counter and is described in Section 4.2.

4.1 Calibration of Ionisation Chamber

The calibration of the ionisation chamber (ION) is performed in order to extract the number of protons per SPS cycle impacting on the H4IRRAD copper target up to beam intensities of the order of 10^9 protons. The procedure is to relate the ION counts to those in the scintillators which already measure the beam intensity in units of p.o.t.. The overlapping linear response of the detectors is exploited for these purposes.

The calibration was performed on June, the 21$^{\text{st}}$ and yield a relation of SCINT coincidence and ION counts as shown in Fig. 8. The linear part comprising data points between 200 and 700 ION counts has been fitted to straight line. The result of that fit is the calibration factor

$$f_{\text{ION}}^{\text{SCINT}} = 6600 \pm 10\ \% \text{ p.o.t. per ION count}$$

This procedure was repeatedly performed during the two operation periods. A relative fast degradation of the scintillator response was observed exhibiting a decreasing slope between ION and SCINT counts. From the initial factor of 6600 p.o.t./ION count, values like 6300 p.o.t./ION count and 5300 p.o.t./ION count were measured with only a short time distance in between them.

Table 3: Cross-check of ION counts with BLM data for two different time periods. Units and the factor of 10^8 are neglected in the ratios.

detector	measurements in June	measurements in July
ION [10^8 protons/spill]	9.47	9.05
hBLM [mGy/spill]	10.3	9.9
vBLM [mGy/spill]	3.7	3.6
ratio ION/hBLM	0.919	0.914
ratio ION/vBLM	2.559	2.514

Due to the relative rapidly changing relation between ION and SCINT over time, several cross-checks were performed which strengthened the hypothesis that the reason of the decreasing slopes is the aging of the scintillators caused by the cumulative received dose. One such cross-check consisted in relating the dose measured in the BLMs to the ION counts for several time periods in June and July. The comparison with BLM data in Table 3 shows that the relation is constant within the given statistics. This gave rise to the assumption that the ION was performing as expected while the scintillators did not show nominal performance. As consequence, they will be replaced for the upcoming irradiation periods. Since the beam intensity is a crucial quantity to evaluate radiation levels and doses a further calibration was required and performed using the PIC.

4.2 Calibration with PIC Counter

In order to use the PIC to measure the number of protons, $N_{\text{p.o.t.}}$, two calibrations have been performed. First, an absolute calibration using an activation technique was performed which relates a count in the PIC to the $N_{\text{p.o.t.}}$. This had been measured at CERF [17] and was repeated for the H4IRRAD area. Once, this relation is established a cross-calibration was made to determine the relation between ION and PIC counts. This gave a cross-check of the ION calibration using SCINT counts.

4.2.1 Calibration of PIC in H4IRRAD with Aluminum foil activation

An activation experiment with calibrated Aluminum (Al) foils was performed on July, 9^{th} 2011 in order to verify the calibration factor for the PIC, relating the number of particles traversing the chamber to the PIC counts. In an earlier experiment [18], the PIC was calibrated for a proton beam of 120 GeV, however using scintillators, to yield

$$(22\ 120 \pm 90) \text{ p.o.t. per PIC count.}$$

The technique of activating aluminum foils by high-energy protons is a convenient method of measuring beam intensity which has been extensively used. The technique consists in revealing the photon (γ) induced activity of the ^{24}Na produced in the Al foils by the activation reactions ^{27}Al(p,x)^{24}Na. The short half-life of ^{24}Na results in a high specific activity so a relatively low irradiation time is adequate to obtain a reasonable activity. A detailed description of the activation experiment performed at H4IRRAD and at CERF can be found in [17]. The result from the experiment at H4IRRAD yield a calibration factor of

$$(21\ 210 \pm 950) \text{ p.o.t. per PIC count}$$

and is in well agreement to the previously obtained calibration value. The full data analysis of the Al activation experiment is being completed and taking into account serval sources of uncertainties

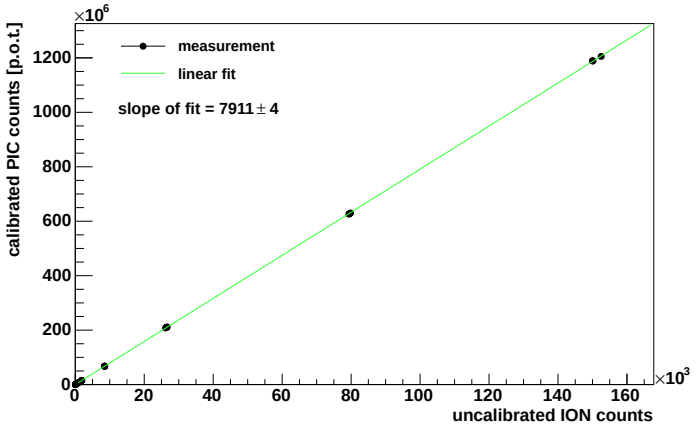

Figure 9: Calibration of ionisation chamber counts with the PIC counter in the beginning of the 2nd irradiation slot (July 12th).

the value is slightly revised to (22 500 $\pm$ 2 200) p.o.t./PIC count. For the purposes described in this note, the first result is used for the cross-calibration between the PIC and ION.

4.2.2 Cross-calibration between PIC and ION

For the H4IRRAD beamline, a cross-calibration between PIC and ION was performed on July 12th 2011 with the PIC installed around seven meters downstream of ION. The beam intensity was varied in eight steps starting with about 10^5 up to 10^9 protons per spill. Several measurements were performed each time the intensity was varied by changing the collimator settings downstream of T2. Using the previously obtained calibration factor of (21 210 $\pm$ 950) p.o.t. per PIC count, the ION counts are calibrated to yield the number of protons, $N_{\text{p.o.t.}}$. The relation between the beam intensity measured with the PIC and the ION counts is shown in Fig. 9. The linear region comprising data points between 700 and 150,000 ION counts is fitted to a straight line. Data points at the lowest intensities were not included in the fit as these measurements are affected by background radiation. The calibration factor for the ION counts is estimated to be (7911 $\pm$ 4) p.o.t./ION count. Taking into account the uncertainty on the PIC calibration factor, the corrected estimate for the ION calibration factor was determined to

$$f_{\text{ION}}^{\text{PIC}} = (7900 \pm 400) \text{ p.o.t. per ION count.}$$

An updated calibration factor was extracted during the third irradiation slot and is described in Appendix B.

4.3 Determination of p.o.t.

The number of p.o.t. was obtained by calibrating the ION counts:

$$N_{p.o.t.} = N_{\text{ION}} \times f_{\text{ION}} \tag{1}$$

with N_{ION} being the counts measured in the ionisation chamber and f_{ION} the calibration factor of the ionisation chamber. A difference of 20 % was found for the calibration factor of the ionisation chamber based on the scintillators, $f_{\text{ION}}^{\text{SCINT}}$, and the PIC, $f_{\text{ION}}^{\text{PIC}}$. It was chosen to use the one measured with the PIC counts, since no indication could be obtained whether the number solely obtained

Table 4: Calibration factors $f_{\text{ION}}^{\text{RadMon}}$ for RadMon signals to yield ION counts averaged over four days of irradiation from 14.07. 00:00:00 to 17.07.2011 23:59:59 MEST. Note, only statistical uncertainties are indicated.

detector	$f_{\text{ION}}^{\text{RadMon}}$ [$\times 10^{-6}$ N_{SEU}/counts]
H4RAD01	3.90 ± 0.14 (3.6 %)
H4RAD02	2.63 ± 0.14 (5.5 %)
H4RAD03	6.51 ± 0.60 (9.3 %)
H4RAD04	4.46 ± 0.04 (0.8 %)
H4RAD05	1.12 ± 0.05 (4.4 %)

between SCINT and ION could be correct or not, thus the factor $f_{\text{ION}}^{\text{PIC}}$ = (7900 $\pm$ 400) p.o.t. per ION count was used for f_{ION}.

During the beginning of the second slot in July, there were several issues e.g. the mis-configuration of one magnet in the H4-beamline which prevented the use of the ionisation chamber. An alternative method to obtain N_{ION} for the respective time period was therefore used for the period starting from July, 10^{th}, 00:00:00 to July, 13^{th}, 23:59:59 MEST. During that period RadMon measurements were calibrated to yield ION counts. The calibration factor was obtained from a time period where both, ION and the RadMons were working at nominal conditions. The chosen the time period is from July, 14^{th} to 17^{th}. The calibration factors for each RadMon are listed in Table 4.

For the determination of ION counts during the time the magnet was mis-configured it was chosen to use measurements of RadMon 2, since its position did not change between the 10^{th} and 17^{th} of July. This was also the case of RadMon 5 however that RadMon was located in the external zone and fewer measurements were made compared RadMon 2 in the internal zone. Thus, the factor N_{ION} in Eq. 1 was obtained by scaling the number of SEU counts made by RadMon 2, N_{RadMon2}, with its calibration factor, i.e. $N_{\text{ION}} = N_{\text{RadMon2}}/2.63$.

The final results on the measurements of cumulative number of protons for both irradiation slots are shown in Fig. 10. A total of $12.7 \cdot 10^{12}$ p.o.t. and $19.4 \cdot 10^{12}$ p.o.t. was delivered in the 1^{st} and 2^{nd} irradiation period, respectively.

5 Calibration of the Radiation Field

By using the measured proton/spill impinging on the H4IRRAD target, FLUKA simulations are used to predict the high energy hadron (HEH) and thermal neutron fluences as well as the deposited doses in the specific locations. Two studies are described in the following comparing simulated dose values and fluences with measurements using RadMon and BLM data.

5.1 Comparison of High-Energy-Hadron and thermal Neutron Fluences with RadMon Measurements

RadMons, based on SRAM memory device, are used as Single Event Upset (SEU) monitors. Their response on SEU is described in Eq. 2

$$N_{\text{SEU}} = \sigma_{\text{th.n}} \cdot \Phi_{\text{th.n}} + \sigma_{\text{HEH}} \cdot \Phi_{\text{HEH}} \tag{2}$$

where σ and Φ denote the failure cross-section and fluence of thermal neutrons (th.n) or high energy hadrons (HEH), respectively. The cross-sections depend on a voltage bias of the detector and were

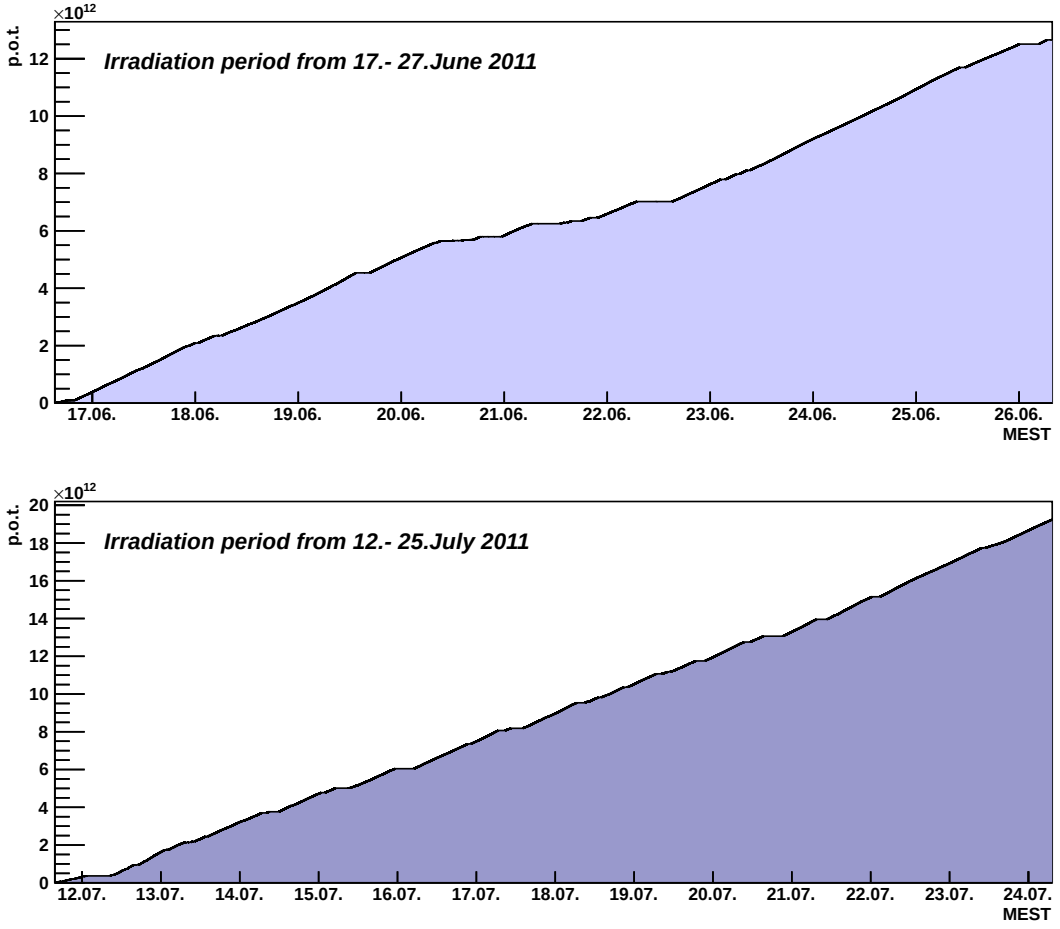

Figure 10: Measured number of protons (p.o.t.) for the first two irradiation periods at H4IRRAD. A total of 12.7·10^{12} p.o.t. was delivered in the 1st period which was slightly increased with 19.4·10^{12} p.o.t. in the 2nd irradiation period.

Table 5: Comparison of measured (by RadMons) and simulated (FLUKA) HEH and thermal neutron fluences, Φ_{HEH} and $\Phi_{\text{th.n}}$, during the first irradiation slot.

detector	measurement	simulation	sim./meas.
	Φ_{HEH} [10^{-3}/p.o.t./cm^2]		
H4RAD01	0.37 ± 0.16 (43 %)	0.32 ± 0.01 (1.3 %)	0.85 ± 0.37 (44 %)
H4RAD02	0.37 ± 0.16 (43 %)	0.36 ± 0.01 (1.7 %)	0.98 ± 0.43 (44 %)
H4RAD03	3.93 ± 1.69 (43 %)	4.78 ± 0.02 (0.4 %)	1.22 ± 0.53 (43 %)
H4RAD04	1.89 ± 0.81 (43 %)	1.65 ± 0.01 (0.7 %)	0.87 ± 0.38 (44 %)
H4RAD05	0.69 ± 0.30 (43 %)	0.69 ± 0.01 (1.1 %)	1.00 ± 0.43 (43 %)
	$\Phi_{\text{th.n}}$ [10^{-3}/p.o.t./cm^2]		
H4RAD01	0.99 ± 0.43 (43 %)	2.90 ± 0.01 (0.5 %)	2.9 ± 1.25 (43 %)
H4RAD02	0.95 ± 0.41 (43 %)	2.84 ± 0.01 (0.4 %)	3.0 ± 1.28 (43 %)
H4RAD03	1.15 ± 0.49 (43 %)	3.04 ± 0.02 (0.6 %)	2.6 ± 1.12 (43 %)
H4RAD04	1.21 ± 0.52 (43 %)	3.29 ± 0.01 (0.4 %)	2.7 ± 1.16 (43 %)
H4RAD05	0.99 ± 0.43 (43 %)	2.87 ± 0.01 (0.5 %)	2.9 ± 1.23 (42 %)

Table 6: Comparison of the number of SEU counts, N_{SEU}, measured by RadMons and calculated from HEH fluence and thermal neutron fluence simulated by FLUKA during the 2^{nd} irradiation slot.

	N_{SEU} [10^{-10} p.o.t.$^{-1}$]				
detector	measurement	simulation	sim./meas.	simulation corr.	sim./meas. corr.
H4RAD01	5.00 ± 1.1 %	5.11 ± 7.7 %	1.02 ± 0.08 (8 %)	4.23 ± 39 %	0.85 ± 0.33 (39 %)
H4RAD02	3.36 ± 1.4 %	4.24 ± 7.7 %	1.26 ± 0.10 (8 %)	3.52 ± 39 %	1.05 ± 0.41 (39 %)
H4RAD03	8.94 ± 0.8 %	1.00 ± 8.5 %	1.12 ± 0.10 (9 %)	9.06 ± 41 %	1.01 ± 0.42 (42 %)
H4RAD04	5.64 ± 1.0 %	6.77 ± 8.0 %	1.20 ± 0.10 (8 %)	5.80 ± 40 %	1.03 ± 0.41 (40 %)
H4RAD05	1.53 ± 2.0 %	3.34 ± 7.2 %	2.18 ± 0.16 (7 %)	2.45 ± 36 %	1.60 ± 0.58 (36 %)

taken from [14]. Two different comparisons were made, using data of the first and second irradiation period.

For the first irradiation slot, the number of SEU responses, N_{SEU}, were measured for all five RadMons and both biases. The fluences Φ_{HEH} and $\Phi_{\text{th.n}}$ were extracted using the respective cross-sections from [14]. The measured and simulated fluences are normalised per proton on target and their comparison are presented in Table 5.

For the second irradiation slot, the measured number of SEU is compared to the calculated number using Eq. 2. Φ_{HEH} and $\Phi_{\text{th.n}}$ are taken from simulation and the respective cross-sections from [14]. These are used to compute N_{SEU}. The results and their comparison to measured N_{SEU} are presented in Table 6. This table shows in addition *corrected* simulated values. They were obtained by correcting the simulated values for Φ_{HEH} and $\Phi_{\text{th.n}}$.

As as Table 5 shows, the simulated values of Φ_{HEH} are slightly underestimated while $\Phi_{\text{th.n}}$ are overestimated by a factor 2 to 3 when comparing to the data. With an average value for the under- and overestimation, the simulation is corrected. A much better agreement is obtained when the corrected simulated values are compared to the measurements as can be seen from Table 6. The uncertainties for the calculated values in both tables are mainly due to about 10 % uncertainty of the SEU cross-section measurements.

However, the measurement of N_{SEU} by RadMon 5 remains to be quite different from the simulation where the measured value is significantly smaller than the simulated one. This can be explained by the additional attenuation from the material in front of RadMon 5 that is not included in the simulation.

5.2 Comparison of Simulated Doses with BLM Measurements

The dose at the positions of both BLMs were simulated with FLUKA and compared to measurements. The measured dose corrected for the time-dependent offset of each BLM has been integrated over different time periods. These time periods were chosen when data-acquisition and beam conditions were operating at nominal parameters. During these time intervals, the ratio of the measured cumulative dose and cumulative $N_{\text{p.o.t.}}$ is formed. The simulations yield for the dose $4.12 \cdot 10^{-12}$ Gy/p.o.t. and $10.3 \cdot 10^{-12}$ Gy/p.o.t. for the vertical and horizontal BLM, respectively. The comparisons to the measurements are summarised in Table 7.

One can observe that the FLUKA simulations of the horizontal BLM agree relatively well with the measurements, however with a systematic shift in the 2^{nd} irradiation period of around 10 %. A similar situation is observed for the vertical BLM data of the 1^{st} slot when they lie systematically around 10 % to 20 % below the simulation. The discrepancy is as for the horizontal BLM data also systematically shifted in the 2^{nd} slot. The deviations of simulated and measured values for the second

Table 7: Comparison of simulated and measured doses using both BLMs. Periods for both irradiation slots were chosen. Statistical uncertainties were negligible and are not indicated.

duration [hours]	$N_{\text{p.o.t.}}$ [10^{12}]	hBLM [Gy]	vBLM [Gy]	hBLM/$N_{\text{p.o.t.}}$ [Gy/10^{12}p.o.t.]	vBLM/$N_{\text{p.o.t.}}$ [Gy/10^{12}p.o.t.]	sim/meas. hBLM	sim./meas. vBLM
1st irradiation slot							
5	0.137	1.40	0.50	10.22	3.65	1.01	1.13
15	1.13	11.02	3.94	9.75	3.48	1.06	1.18
48	2.973	30.92	11.07	10.40	3.72	0.99	1.11
30	2.164	20.61	7.54	9.52	3.48	1.08	1.18
2nd irradiation slot							
37.2	1.03	9.16	3.34	8.90	3.24	1.16	1.27
65.4	2.20	19.77	7.16	9.00	3.26	1.15	1.26
40.1	1.31	12.44	4.50	9.48	3.43	1.09	1.20
21.2	0.90	8.42	3.05	9.39	3.40	1.10	1.21

slot likely relates to the longer time period in which the BLM dose was cumulated and being more affected by possible uncertainties due to offset correction. Furthermore, it is possible that the vertical BLM encounters some additional attenuation of fluences as the horizontal BLM and the installation material is placed directly in front of the vertical BLM. This additional material was not considered in the simulation.

5.3 Determination of Doses, High-Energy-Hadron and thermal Neutron Fluences at Test Locations

Power converters and various other equipment were irradiated during both slots. The positions of the equipment are depicted in Fig. 11. Simulation of cumulated doses, high energy hadron fluence Φ_{HEH}, thermal neutron fluence $\Phi_{\text{th.n}}$ and neutron equivalent fluence Φ_{neq} averaged over the tested equipment volumes are shown in Table 8 with statistical uncertainties.

The measured mixed-field components were obtained by scaling to the measured number of p.o.t., for example the measured HEH fluence $\Phi_{\text{HEH}}^{\text{meas}}$ is $\Phi_{\text{HEH}}^{\text{meas}} = \Phi_{\text{HEH}} \cdot N_{\text{p.o.t.}}$. Respective uncertainties were determined in following way:

- Φ_{HEH}: Considering the agreement of RadMon measurements and FLUKA simulations as discussed in Section 5.1 and the uncertainty of RadMon devices to count an SEU being around 40 %, an uncertainty of $\pm$50 % is assigned to the measured Φ_{HEH}.
- $\Phi_{\text{th.n}}$: A correction factor of 2.5 is applied to account for the overestimated simulated thermal neutron fluences when compared to data, see Table 6. An uncertainty of $\pm$50 % is considered here as well.
- Dose: Due to relative large uncertainties of the RadFETs a factor $\times$2 is assigned as uncertainty.

It is necessary to take into account that especially in the internal testing position, the field gradient can have a rather strong influence depending on a location and an equipment size. This has been investigated for Φ_{HEH} at all the test locations.

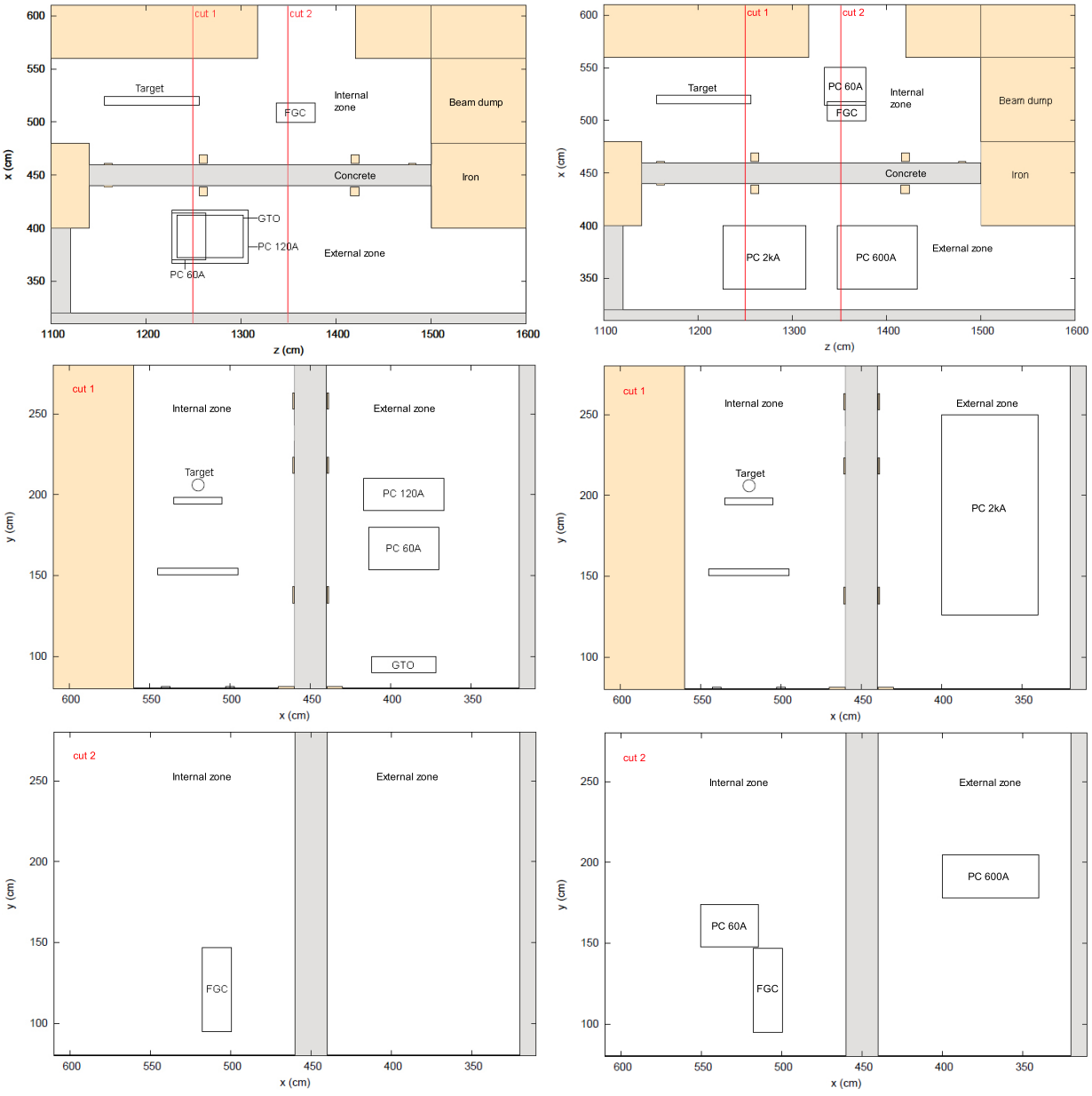

Figure 11: Top and side views (cut 1 and cut 2) on equipment position during the first (left column) and second (right column) irradiation slot.

Table 8: Simulated radiation field in the testing positions during the first and second irradiation slots with statistical uncertainties.

LHC equipment	1st irradiation slot FGC *int*	GTO *ext*	PC60A *ext*	PC120A *ext*
dose [10^{-13} Gy /p.o.t.]	8.63 ± 0.4 %	1.05 ± 1.5 %	2.17 ± 1.1 %	2.43 ± 0.7 %
$\Phi_{\text{HEH}}[10^{-3}/\text{p.o.t./cm}^2]$	1.49 ± 0.2 %	0.30 ± 0.5 %	0.63 ± 0.2 %	0.70 ± 0.3 %
$\Phi_{\text{th.n}}[10^{-3}/\text{p.o.t./cm}^2]$	3.21 ± 0.1 %	2.81 ± 0.2 %	3.15 ± 0.2 %	3.05 ± 0.1 %
$\Phi_{\text{neq}}[10^{-3}/\text{p.o.t./cm}^2]$	7.71 ± 0.1 %	1.44 ± 0.2 %	2.69 ± 0.2 %	2.80 ± 0.2 %
LHC equipment	2nd irradiation slot FGC *int*	PC2kA *ext*	PC60A *int*	PC600A *ext*
dose [10^{-13} Gy /p.o.t.]	8.59 ± 0.5 %	1.78 ± 0.3 %	11.7 ± 0.4 %	1.89 ± 0.7 %
$\Phi_{\text{HEH}}[10^{-3}/\text{p.o.t./cm}^2]$	1.48 ± 0.2 %	0.48 ± 0.2 %	2.12 ± 0.2 %	0.47 ± 0.3 %
$\Phi_{\text{th.n}}[10^{-3}/\text{p.o.t./cm}^2]$	3.21 ± 0.1 %	2.93 ± 0.1 %	2.72 ± 0.2 %	2.32 ± 0.1 %
$\Phi_{\text{neq}}[10^{-3}/\text{p.o.t./cm}^2]$	7.69 ± 0.1 %	2.18 ± 0.1 %	8.54 ± 0.1 %	1.63 ± 0.2 %

Table 9: FLUKA simulated field gradient of Φ_{HEH} for equipment tested during both slots. The fluence variations $\Delta\Phi_{\text{HEH}}$ are indicated relative to the averaged fluence Φ_{HEH}.

LHC equipment	1st irradiation slot FGC *int*	GTO *ext*	PC60A *ext*	PC120A *ext*
$\Phi_{\text{HEH}}[10^{-3}/\text{p.o.t./cm}^2]$	1.49	3.02	0.63	0.70
$\Delta\Phi_{\text{HEH}}$ in x [%]	$\pm\,^{7}_{0}$	$\pm\,^{4}_{9}$	$\pm^{29}_{13}$	$\pm^{27}_{22}$
$\Delta\Phi_{\text{HEH}}$ in y [%]	$\pm^{36}_{17}$	$\pm\,^{4}_{9}$	$+^{14}_{2}$	$-^{11}_{12}$
$\Delta\Phi_{\text{HEH}}$ in z [%]	$\pm^{15}_{3}$	$\pm^{10}_{0}$	$+\,^{11}_{5}$	$\pm\,^{6}_{7}$
LHC equipment	2nd irradiation slot FGC *int*	PC2kA *ext*	PC60A *int*	PC600A *ext*
$\Phi_{\text{HEH}}[10^{-3}/\text{p.o.t./cm}^2]$		0.48	2.12	0.47
$\Delta\Phi_{\text{HEH}}$ in x [%]	as in	$\pm^{32}_{0}$	$\pm\,^{1}_{8}$	$\pm^{27}_{20}$
$\Delta\Phi_{\text{HEH}}$ in y [%]	1st slot	$\pm^{23}_{32}$	$\pm\,^{3}_{15}$	$\pm\,^{2}_{0}$
$\Delta\Phi_{\text{HEH}}$ in z [%]		$\pm\,^{4}_{8}$	$\pm^{18}_{18}$	$\pm\,^{9}_{4}$

5.4 Field Gradients within Equipment Volume

The field gradient of Φ_{HEH} was investigated within the volume of the different equipment locations as visualised in Fig. 11. The variations of Φ_{HEH}, $\Delta\Phi_{\text{HEH}}$, in three dimensions x, y and z are shown in Table 9. They are indicated relative to the averaged fluence Φ_{HEH} with the "+"-sign indicating the maximal deviation and the "−"-sign the minimal deviation from the averaged fluence Φ_{HEH}. This analysis shows that strong gradients should be expected in the internal zone e.g. at the position of the FCG along the height in y and in the external zone along x. For the PC2kA in the external zone the total gradient in x was verified with RadMon measurements. First indications of material suppression were already discussed in Section 5.1. RadMon 1 was placed on the front-side of the rack, while RadMon 5 was mounted on the back-side at the same height. At the front-side the measured SEU counts is 32 % higher than at the back-side, measured over from 15^{th} of July until the end of the second irradiation slot. When comparing to the simlated field gradient, a decrease by around 12 % is found. This suggests that 20 %, the difference of the remaining measured suppression of Φ_{HEH}, is caused by the material of PC2kA.

6 Summary and Conclusion

A new test area has been setup for systematic testing of bulk LHC equipment. It has successfully been commissioned in June 2011. During two irradiation periods, various equipment was tested in an LHC tunnel- and shielding-like environment. The mixed-fields have been calibrated using different detectors, the PIC and the SPS ionisation chamber ION. The different field components were simulated with FLUKA and compared to measurements obtained from RadMons and BLMs. Comparisons of measured and simulated thermal neutron fluences as listed in Table 5 show a systematic overestimation of the thermal neutron fluence in the simulation. High energy hadron fluences are relatively well reproduced, however the total uncertainty of the comparisons of both fluence types is around 40 %. A total of $12.7 \cdot 10^{12}$ p.o.t. was delivered in the 1^{st} period, which was slightly increased in the 2^{nd} irradiation period with $19.4 \cdot 10^{12}$ p.o.t.. The equipment users could thus estimate failure rates of their device, which is crucial for continuing the successful performance of the LHC.

Further irradiation periods are scheduled in which other devices are stressed probing their lifetime performance within a few days of irradiation.

Acknowledgments

The authors would like to thank the EN/MEF Group for the great support during the construction of the test area as well as during the installation and dismantling operations in each irradiation slots. Warm thanks to EN/CV for the preparation of the water cooling circuits and well as to DGS/RP and BE/BI for, respectively, the radiation and beam monitoring devices. A special thanks to all the groups who contributed to the success of the test campaigns, TE/EPC, TE/ABT, EN/EL and EN/ICE. Finally we would like to acknowledge all the experiments in the North Area, which allowed the accommodation of the H4IRRAD tests during 2011. H4IRRAD is operated and the tests are coordinated by the EN/STI Group, which also provides the RadMon monitoring system.

A Appendix RadMon Positions

The positioning of the five RadMons in six vertical cuts as indicated in Fig. 7 (b) are shown in Fig. 12.

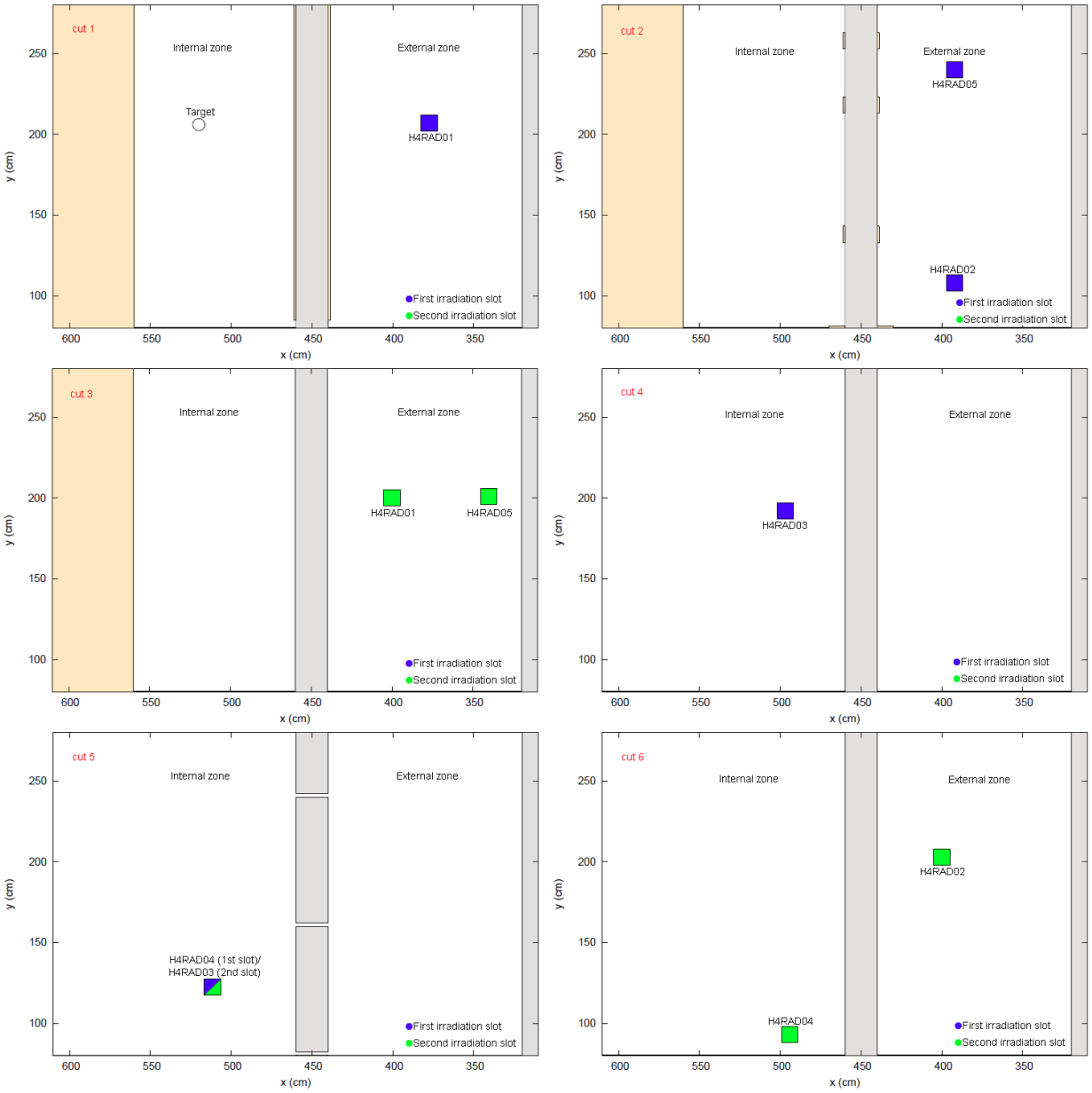

Figure 12: Side views (cut 1 to 6) of RadMons positions located in the internal and external zone during the first (blue) and second (green) irradiation period.

B Appendix POT Calibration with new ION

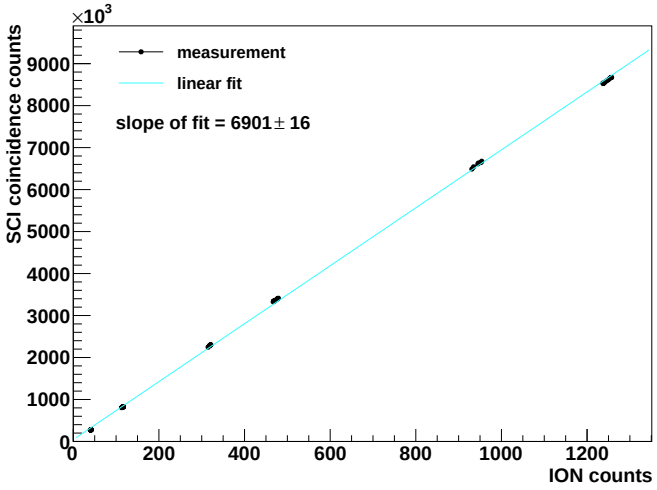

Figure 13: Calibration of ION using scintillator coincidence counts (both background substracted). The indicated uncertainty is from the fit only and does not include any systematic uncertainties. For final calibration, see text.

As mentioned in Section 4.1 and 4.2 the calibration of the ionisation chamber ION during the first two H4IRRAD slots in 2011 was performed based on the PIC counter only due to the degrading performance of the scintillators (SCINT). Before the third slot in October 2011 started, these scintillator detectors were replaced and a new, final calibration for 2011 between ION and SCINT could be obtained. This appendix describes this final calibration which should be used for analyses depending on the p.o.t. determination.

The procedure of the calibration is the same as described in Section 4.1. The data used were recorded 18.10.2011 during about two hours. The counts of ION and the scintiallator coincidence were both background corrected. The background was determined from periods in which no beam was present yielding a background substraction of 4 counts of the recorded ION counts and 48 of the SCINT coincidence counts. The linear response region ranging from 0 to about 1300 ION counts was considered for the calibration. This is shown in Fig. 13 indicating as well the fit result of the data. Two sources of systematic uncertainty were considered: the first one is obtained from a p.o.t. calibration by the PIC which was estimated to be around 5 % (as described in Section 4.2). The second source takes into account an uncertainty of the absolute calibration of the scintillators estimated be around 8 % such that the final calibration factor becomes

$$f_{\mathrm{ION}}^{\mathrm{SCIN}} = 6900\ p.o.t.\ \text{per ION count} \pm 10\ \% \tag{3}$$

With this conservative uncertainty the previously obtained value for the p.o.t. calibration factor of (7900 $\pm$ 400) is covered. Tentative results of the PIC calibration during the third irradiation slot are in good agreement with the value from Eq. 3 [19].

References

[1] www.cern.ch/r2e

[2] M. Brugger and M. Calviani, *H4IRRAD a radiation test area for LHC equipment*, EDMS No.1145469, May 2011.

[3] https://espace.cern.ch/h4irrad/default.aspx

[4] M. Brugger et al., *H4IRRAD Test Area Operation*, EDMS No.1140720, May 2011.

[5] http://radwg.web.cern.ch/RadWG/Pages/CNRAD/cnrad_frame.htm

[6] A. Ferrari, P. Sala, A. Fasso and J. Ranft, *FLUKA: A multi-particle transport code*. CERN-2005-10(2005), INFN/TC_05/11, SLAC-R-773

[7] B. Biskup, M. Calviani, M. Brugger, I. Efthymiopoulos, *H4IRRAD General Studies*, ATS note to be published (2011)

[8] I. Efthymiopoulos, *H4IRRAD Test Area in the EHN1 for LHC Components - Discussion on Intensity*, EDMS 1151181, June 2011.

[9] D. Forkel-Wirth and T. Otto, *Area Classification*, EDMS 810149, 2006.

[10] G. Spiezia et al., *The LHC accelerator Radiation Monitoring System - RadMON*, Conference Proceedings, to be published in PoS, 2011.

[11] V. Agoritsas, *A Sealed Metal Argon Ionization Chamber (Argonion)*, IEEE Transactions on Nuclear Science, Vol. NS–28, No. 3, 1981

[12] A. Mitaroff and M. Silari, *The CERN-EU High-Energy Reference Field (CERF) Facility For Dosimetry At Commercial Flight Altitudes And In Space*, Radiation Protection Dosimetry, **102**:7–22, CERN-TIS-2001-006-RP-PP, 2002.

[13] F.P. La Torre, G.P. Manessi, F. Pozzi, C.T. Severino, M. Silari, *The June 2011 CERF run*, CERN Technical Note, CERN/DGS/2011-055/RP/TN, 2011.

[14] K. Roeed et al., *FLUKA Simulations for SEE Studies of Critical LHC Underground Areas*, IEEE Transactions on Nucl.Science, **58**, No.3, June 2011.

[15] C. Zamantzas et al., *The LHC Beam Loss Monitoring System Commissioning for 2010*, Workshop Proceedings, January 2010.

[16] T. Wijnands et al., *On line radiation monitoring for the LHC and experimental cavern*, Workshop Proceedings, September, 2006.

[17] F.P. La Torre, G.P. Manessi, F. Pozzi, C.T. Severino, M. Silari, *Al activation experiment for the calibration of the CERF beam monitor*, CERN-DGS-2011-071-RP-TN, EDMS 1163587, 2011.

[18] H. Vincke et al., *Accurate PIC calibration by the use of a coincidence of two scintillators*, CERN-SC-2004-090-RP-TN, EDMS 536144, 2004.

[19] F.P. La Torre, G.P. Manessi, F. Pozzi, C.T. Severino, M. Silari, *Cu and Al activation experiments for beam monitoring in H4IRRAD*, 2012 (to be published).